Reduced surface magnetization of NiMnSb(001)

H. Kolev, G. Rangelov, J. Braun, and M. Donath

Physikalisches Institut, Westfälische Wilhelms-Universität Münster, Wilhelm-Klemm-Strasse 10, D-48149 Münster, Germany

The spin-dependent electronic structure at the (001) surface of the ferromagnetic half-Heusler alloy NiMnSb has been investigated by spin-resolved appearance potential spectroscopy. This surface-sensitive technique provides access to the spin- and element-resolved local density of unoccupied states and, therefore, probes the spin polarization above the Fermi level. In combination with low-energy electron diffraction and magneto-optical Kerr effect measurements, we characterized the sample with respect to its crystal structure, electronic structure, and magnetic properties. Our spectroscopic experiments were accompanied by a quantitative theoretical analysis. The theoretical appearance potential spectra are based on self-consistent electronic structure results for the bulk. They have been obtained in a fully relativistic framework as a self-convolution of the matrix element-weighted, orbitally resolved unoccupied density of states. The spin asymmetry in the experimental results, obtained from the surface region, is found to be significantly reduced compared with the calculations based on the bulk electronic structure of NiMnSb. Possible reasons for the reduced surface magnetization are discussed.

PACS number(s): 75.70.Rf, 71.20.Gj, 75.50.Cc, 78.70.−g

I. INTRODUCTION

In the last decade, the magnetoelectronics has emerged as an important further development of the microelectronics.[1,2] The physics behind this development is spin-polarized electron transport. Materials with spin diffusion lengths comparable to the device dimensions are needed. In this respect some Heusler alloys are possible candidates. Heusler alloys are ternary cubic phases X_2YZ (Heusler alloys) or XYZ (half-Heusler alloys) where $X = \text{Ni}, \text{Co}, \text{Pt}, \ldots$, $Y = \text{Mn}, \text{Sr}, \ldots$, and $Z = \text{Sb}, \text{As}, \ldots$.[3] Band-structure calculations predicted some ferromagnetic (half-)Heusler alloys[4,5] to be half metals. This means that at the Fermi level E_F no minority electronic states exist, whereas the majority states show metallic behavior. For example, de Groot *et al.*[5] predicted for NiMnSb a 0.5 eV band gap for the minority electrons at E_F and therefore a 100% spin polarization at the Fermi level. However, no experimental proof of 100% spin polarization at E_F in the case of NiMnSb has been presented yet. Bulk sensitive methods like spin-resolved positron annihilation,[6] neutron scattering,[7] and infrared reflection spectroscopy[8] support the half metallic character of NiMnSb. On the other hand, using interface sensitive methods like Andreev-reflection[9] or surface sensitive methods like spin-resolved photoemission[10] spin polarizations of only $\approx 50\%$ were observed. One study by angle and spin-resolved inverse photoemission reported close to 100% spin polarization at E_F and $\bar{\Gamma}$.[11] Until now, however, there exist no systematic studies of the spin-resolved electronic structure $E_{\uparrow,\downarrow}(\mathbf{k})$ of single-crystalline NiMnSb samples. It was suggested that the disagreement between the bulk sensitive and surface (interface) sensitive methods is due to surface (interface) defects like structural and/or chemical disorder which cause specific surface (interface) electronic states.[12–14] Electronic defect states in the minority band gap are expected to reduce the spin polarization at E_F. Another possible reason for the reduced polarization at surfaces and interfaces might be a reduced magnetization com-

pared with the bulk. No experimental proof of this hypothesis exists so far.

In this paper, we studied the (001) surface of a NiMnSb single crystal with a combination of techniques able to characterize surface structure and composition as well as magnetic order and electronic structure. We used low-energy electron diffraction (LEED) to test the crystallographic order and Auger-electron spectroscopy (AES) for compositional analysis of the surface. The sample magnetization was checked by *extra situm* and *in situ* magnetooptical Kerr effect (MOKE) measurements as well as *extra situm* Kerr microscopy. To reveal the electronic structure, we applied spin-resolved (SR) appearance potential spectroscopy (APS). This is an element-specific, surface and magnetically sensitive technique able to provide element-specific information about the spin-dependent electronic states above the Fermi level. We note, however, that APS is not particularly sensitive to details of the electronic structure in the vicinity of E_F. We concentrated on the Mn threshold because the Mn magnetic moment (3.79 μ_B) is much higher than the Ni magnetic moment (0.18 μ_B)[15] and, therefore, a larger spin asymmetry is expected in the experimental AP signal. Our measurements are accompanied by a quantitative theoretical analysis of the AP spectra.

II. TECHNICAL DETAILS

A. Experiment

Our investigations on NiMnSb(001) were performed in an ultra-high vacuum (UHV) system with a base pressure of about 5×10^{-11} mbar. The UHV system consists of two chambers. The main chamber, used for sample preparation and characterization, is equipped with LEED, AES (four-grid retarding-field electron analyzer), and longitudinal MOKE. This chamber also contains the soft x-ray (SX) detector for APS.[16] A GaAs photocathode as a source for spin-polarized

electrons[17,18] is installed in a second chamber. Both chambers are connected by an electron transfer optics[17] which transports the electron beam from the electron source to the sample.

The NiMnSb surface was prepared using a sputter/anneal procedure described in Sec. III. The sample temperature was measured with a nonmagnetic thermocouple type D -$W_{0.97}Re_{0.03}/W_{0.75}Re_{0.25}$, directly connected to the sample. The surface stoichiometry and surface order were controlled by AES and LEED. The magnetic properties were characterized by longitudinal MOKE with an information depth of ≈ 200 Å. Therefore, it is sensitive to the magnetic (closure) domains within a surface region much thicker than the surface layers probed by electron spectroscopies. The magnetic field was applied along the [110] crystallographic direction of the sample. The field was generated by two coils located outside the vacuum. Each of them consists of a core, embedded in a solenoid. The core and the pole shoes are made of commercial FeCo alloy—VACOFLUX 50 (VAKUUM-SCHMELZE). The shape of the pole shoes was optimized to provide a homogeneous magnetic field with induction up to 825 G at 10 A solenoid current in the middle of the gap between the pole shoes. The main advantage of this construction is that the solenoids are located outside the vacuum, thereby improving the possibilities of cooling in order to reach higher fields.

For APS, the sample is bombarded with electrons of variable energy while the total yield of emitted x rays or electrons is monitored. At energies high enough to excite a core electron (E_c) into empty states above the Fermi level E_F, the yield of emitted particles increases due to the recombination of the created core hole via x-ray or Auger electron emission. Since both the exciting and the excited electrons are scattered into empty states, the rates of possible excitations and, thereby, of detected recombinations depend on the density of states above E_F. The elemental resolution results from the fact that a core level with an element-specific binding energy is involved. Due to the localized character of the core excitation, APS probes the local density of states (LDOS), i.e., the DOS projected onto the excited atom. In our case, we probed the LDOS at the Mn atom within NiMnSb. The surface sensitivity is a result of the short mean free path of the electrons in the solid for the energies in use (8–10 atomic layers for Mn2p excitation energy of ~640–650 eV). In our experimental setup, the APS signal is detected via soft-x-ray emission. The detector arrangement consists of a multichannel plate and a filter with a CsI layer acting as a photon-to-electron converter. For further details see Ref. 19. The APS signal is superimposed on a huge background. Therefore, modulation and lock-in technique have been applied. The first derivative of the APS signal is measured as a function of the primary electron energy E_P. The photocathode potential was modulated by a sine voltage with a peak-to-peak amplitude $V_{pp}=2.0$ eV. This value guarantees a reasonably high APS signal without modulation-dependent broadening. The overall energy resolution is about 1.4 eV full width at half maximum (FWHM).

With the use of spin-polarized electrons APS becomes a magnetically sensitive technique, because the number of empty states in a ferromagnet depends on the spin orientation relative to the magnetization direction. The spin-polarized electron beam used for excitation is emitted from a GaAs photocathode irradiated with circularly polarized 830 nm laser light. In general, the primary energy of the electrons used for excitation is given by $E_P=eU+\Phi_C$, where U is the potential between the cathode and the sample and Φ_C is the cathode work function. In our case, we used a photocathode with negative electron affinity and the relevant number is 1.4 eV, as determined from inverse photoemission data.[20,21] This arrangement provides about 30% longitudinal spin polarization of the emitted electrons.[17] This value is routinely achieved and controlled by the APS asymmetry of standard samples like Fe/Cu(001) and Co/Cu(001). Electrostatic deflection by 90° changes the spin polarization of the electron beam from longitudinal to transversal. The spin asymmetry of the APS signal is given by the normalized difference between the detected signals for electron spin polarization antiparallel and parallel to the magnetization direction of the sample: $A=(I_\uparrow-I_\downarrow)/(I_\uparrow+I_\downarrow)$. A is proportional to the scalar product of the sample magnetization and the electron polarization. In our case, the directions of electron polarization and magnetic field to magnetize the sample are collinear to a $\langle 110 \rangle$ crystallographic direction of the NiMnSb(001) sample. The spectra shown have been renormalized to 100% hypothetical beam polarization. Typical beam currents were 25–30 μA.

B. Theory

For a quantitative analysis of the experimental APS spectra we calculated the AP intensities.[22] Here, we restrict ourselves to a short description of the computational details. Explicit evaluation of the APS intensity leads to

$$I_\sigma(E) \propto \int_0^{E+E_c} dE' \sum_{\kappa\mu\kappa'\mu'} n_{\kappa\mu}(E')n_{\kappa'\mu'}(E+E_c-E')$$
$$\times W^\sigma_{\kappa\mu,\kappa'\mu'}(E',E+E_c-E'). \qquad (1)$$

In Eq. (1) the partial densities of states are denoted by $n_{\kappa\mu}$, where the indices κ,μ denote the usual relativistic quantum numbers. The variety of angular and radial matrix elements is represented by the spin-dependent effective cross section W^σ with σ being the spin index. The intensity itself is given by the weighted self-convolution of the LDOS. This expression is a generalization of the nonrelativistic formula introduced by Hörmanndinger *et al.*[23] for the AES case. Details of the relativistic theory can be found, for example, in Refs. 24 and 25.

The electronic structure of NiMnSb has been calculated by the linear muffin-tin orbitals method[26] in its tight binding implementation.[27] The spin-dependent Mn potential together with the corresponding spin-polarized densities of states serve as input quantities for the spectroscopical analysis, which is described in more detail in Ref. 22. Figure 1(a) shows the LDOS of Mn within NiMnSb. The 100% polarization at E_F results from the gap in the minority channel (dark/red line). The Fermi level is determined by majority states (gray/green line) only and is located at the upper edge of the gap. The unoccupied LDOS is dominated by Mn3d
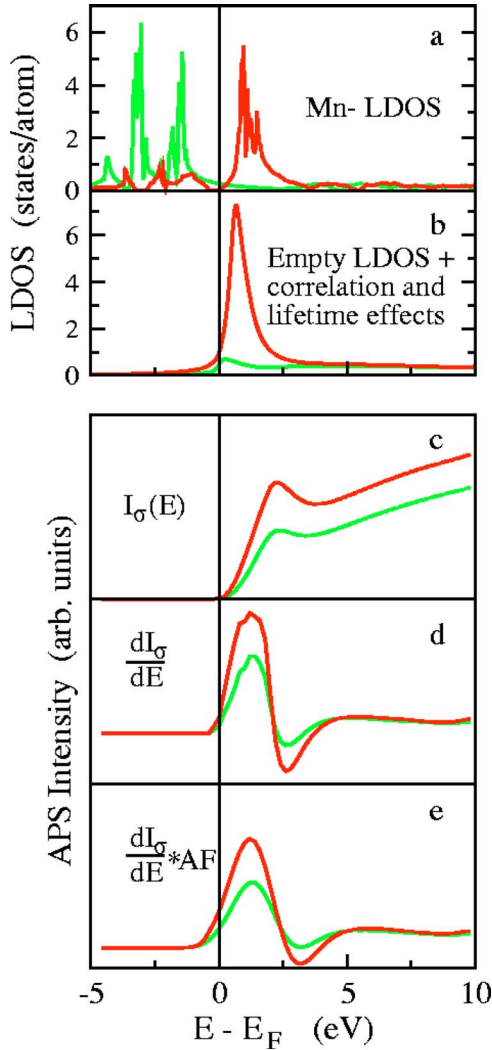
FIG. 1. (Color online) Illustration of the successive steps in the theoretical description of spin-polarized AP spectra of Mn$2p_{3/2}$ in NiMnSb: (a) Majority (gray/green line) and minority (dark/red line) Mn-LDOS. (b) Empty part of the spin-polarized Mn-LDOS corrected for lifetime and correlation effects. (c) Spin-resolved AP intensities $I_\sigma(E)$ calculated from Eq. (1). (d) First derivatives of the majority and minority spectra. (e) Spectra of (d) convoluted with the apparatus function AF.

minority states. There is only a small contribution from majority sp states. As a consequence, one would expect a high spin asymmetry in the Mn AP spectrum.

For a quantitative comparison between the theoretical and the experimental spectra one has to take into account various lifetime effects and the experimental broadening. Electron lifetime effects have been included in our analysis in a phenomenological way using a parametrized complex inner potential $V_o(E) = V_{or}(E) + iV_{oi}(E)$. Herein, the real part serves as a reference energy inside the crystal with respect to the vacuum level. For $V_{oi}(E)$ a constant value $V_{oi} = 30.0$ eV has been chosen. The core-hole lifetime is set to zero.[28] Lifetime effects in the valence-band states are accounted for by using a Lorentzian with an energy-dependent width. In fact we have folded all partial LDOS's with the following Green function:

$$G(E) = \frac{1}{E' - E - i\,\mathrm{Im}\,\sum(E')}. \qquad (2)$$

Herein, Im Σ denotes the imaginary part of the electronic self-energy. The lifetime-broadened LDOS is obtained as the imaginary part of the convolution between the original LDOS and $G(E)$. Similar to valence-band photoemission calculations[29] we decided for an energy dependence of Im Σ, which fulfills some basic requirements. First, the imaginary part of Σ should have a pronounced energy dependence, being proportional to E^2 for energies in the vicinity to E_F.[30] Furthermore, we expect at least a saturation behavior of the contribution of Im Σ that belongs to the Mn$3d$ states in NiMnSb.[31] For all of the other states, which contribute to the APS intensities, we decided for a small constant imaginary part. The following form of Im Σ fulfills the basic requirements, which were discussed above. The explicit parametrization has been chosen to achieve a quantitative agreement with the experimental data. Our optimization procedure results in

$$\mathrm{Im}\,\sum_{\mathrm{Mn}}^{\uparrow\downarrow}(E) = 0.1 + 1.1\arctan(0.1E^2 + 0.03E^4)e^{-0.0005E^2}.$$
$$(3)$$

These values have been taken independent of spin. Additionally, we were forced to consider strong electronic correlations to result in a quantitative agreement between experiment and theory. Strong correlations in the $3d$ states of simple ferromagnetic metals manifest themselves as a renormalization of the one-particle LDOS.[32] Furthermore, correlation effects often lead to energetic shifts in the high-lying electronic states. We tried to account for both in a phenomenological way by scaling all partial unoccupied LDOS's with a factor $\lambda = 0.7(E - E_F)$.

The influence of energy-dependent lifetime broadening and correlation effects on the empty part of the Mn LDOS is demonstrated in Fig. 1(b): the empty LDOS appears at somewhat lower energy. The spin polarization at E_F changes its sign and becomes less than 100%. The calculated APS signal $I_\sigma(E)$ is presented in Fig. 1(c). Due to the self-convolution of the LDOS the maxima are shifted to higher energies and the asymmetry at the Fermi level almost disappears. For reasons of comparison with the experiment, the first derivative of the APS signal was calculated as well [see Fig. 1(d)]. As a consequence of the derivation, the APS peak is transformed into a plus/minus feature and the asymmetry changes sign towards the high energy part. Furthermore, we need to consider the apparatus broadening by convoluting the calculated spectra with a Gaussian of FWHM = 1.4 eV. The theoretical AP spectra finally obtained [Fig. 1(e)] are to be compared with the experimental results.

III. SAMPLE PREPARATION

The preparation of a well-ordered stoichiometric surface of a ternary compound like NiMnSb is not a trivial task. Therefore, we discuss our preparation procedure in detail. The NiMnSb(001) surface was prepared by repeated cycles
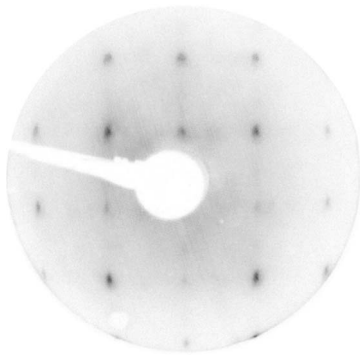
FIG. 2. LEED pattern, taken at 99.8 eV primary electron energy, of NiMnSb(001) with a $c(2\times2)$ superstructure. The horizontal and vertical directions of the figure correspond to $\langle110\rangle$ crystallographic axes.

of sputtering with 1000 eV Ar⁺ ions and prolonged annealing at 700 K. The surface stoichiometry was controlled by AES. For a quantitative analysis of the AES data, we took into account the sensitivity factors of the involved transitions as well as the transmission function of our electron analyzer. We observed that during Ar⁺ sputtering the surface becomes enriched with Ni due to preferential sputtering of Mn and Sb. Subsequent annealing enables Mn and Sb diffusion towards the surface. In consequence, we find a restoration of the bulk stoichiometry at the surface. Based on AES measurements we arrived at a composition ratio of 30:32:38 for Ni:Mn:Sb. The error for each number is estimated to be smaller than 2. Please note that the surface termination, a Mn—Sb layer or a Ni—vacancy layer, influences the observed composition ratio within the limited probing depth of AES. We expect Mn and Sb to appear somewhat stronger in the AES data compared with Ni because a Mn—Sb surface termination is energetically favored. In fact, our data indicate a Mn—Sb terminated surface with some excess Sb. The surface ordering was controlled with LEED. A representative LEED pattern for NiMnSb(001) is shown in Fig. 2. The picture was recorded at 99.8 eV primary electron energy. The LEED pattern demonstrates a clear fourfold symmetry in correspondence with the cubic bulk lattice. The sharpness of the spots and the low background reveal a clean surface with a rather good surface ordering. A closer look shows a $c(2\times2)$ superstructure interpreted as caused by the Ni—vacancy layers with a periodicity different from the Mn—Sb layers. This is a strong indication that the half-Heusler alloy is realized within the surface region. Our preparation as well as characterization results are in good agreement with results within the thesis of Plogmann.[33]

The second important step of the sample preparation is the magnetic characterization. Since the axes of easy magnetization in NiMnSb are of type $\langle111\rangle$,[34] no axis of easy magnetization is expected within the surface plane. A similar case, Ni(001), revealed a complex structure of closure domains at the surface with strongly reduced and even reversed remanent magnetization at the surface.[35] Therefore, we monitored the surface magnetization by *extra situm* Kerr microscopy. A complex domain structure was observed at remanence with domain sizes up to the (sub)millimeter range.
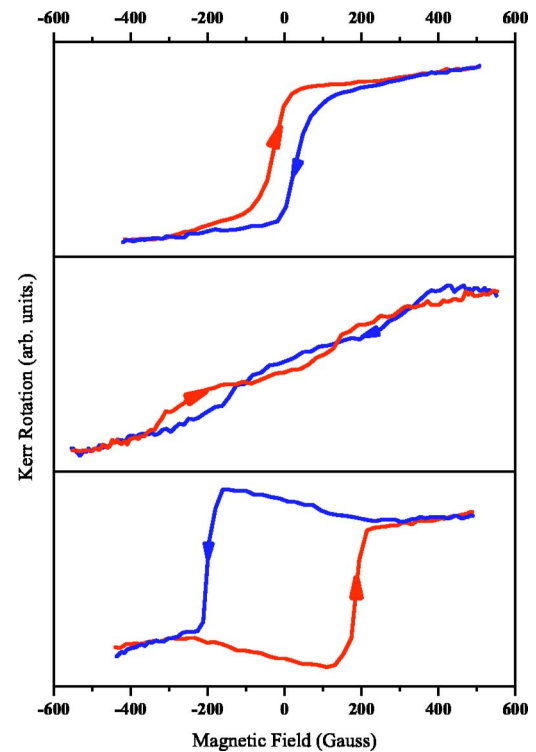
FIG. 3. (Color online) Magnetic properties of NiMnSb(001). Typical longitudinal MOKE hysteresis loops measured at three different locations of the crystal surface. The arrows represent the direction of the magnetic field scan (anti)parallel to the [110] crystal direction.

This observation is supported by *in situ* measurements with longitudinal MOKE. Figure 3 shows three typical hysteresis loops from different regions of the crystal surface. The external magnetic field was aligned parallel or antiparallel to the [110] crystal direction. The arrows represent the direction of the magnetic field scan. The top and the bottom loops exhibit different coercive fields and opposite remanent magnetization. In some cases (middle panel) no clear hysteresis
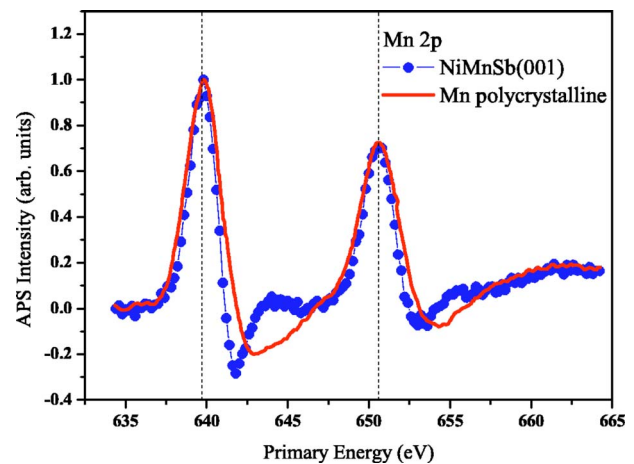
FIG. 4. (Color online) Spin-integrated APS data for NiMnSb(001) at the Mn2p threshold (dots). For reasons of comparison, APS data for polycrystalline Mn are shown as a solid line (Ref. 36).

loop was observed. The mean value of the remanent magnetization obtained by averaging over many regions of the crystal surface accounts to $\approx 56\%$ of the saturation magnetization. Taking into account that the spot diameter of the MOKE laser is ≈ 1 mm, we attribute the different types of loops to a different averaging over differently oriented domains of the MOKE measurement.

IV. RESULTS AND DISCUSSION

Figure 4 shows our spin-integrated APS data for NiMnSb(001) (dots) in comparison with APS data for elemental polycrystalline Mn from the literature (solid line).[36] The spectra have been normalized to equal maximum intensity of the $Mn2p_{3/2}$ line. The chosen energy range comprises the $Mn2p$ threshold. The energy scale gives the primary electron energy as defined above. The APS spectra were measured with a modulation amplitude of 2 V_{pp} for NiMnSb and 1 V_{pp} for polycrystalline Mn. Both spectra show pronounced structures at 639.7 eV from the $Mn2p_{3/2}$ and at 650.5 eV from the $Mn2p_{1/2}$ thresholds. These features originate from the self-convoluted local density of unoccupied d states. The spectral features at the high-energy sides of the main lines for NiMnSb correspond to maxima of the sp-like LDOS, whose appearance and energetic positions are sensitive to the crystallographic order around the atom where the local excitation occurs.[37,38] We observe a rather good overall agreement between the APS data from NiMnSb(001) and those from polycrystalline Mn: The energy positions, the relative intensities of the peak maxima, and the spin-orbit splittings are nearly identical in both cases. But there are differences. The FWHM for NiMnSb is 1.5 eV for $2p_{3/2}$ and 1.7 eV for $2p_{1/2}$. In the case of polycrystalline Mn the corresponding values are 2 and 2.4 eV, although the modulation amplitude is smaller. The larger FWHM in the case of polycrystalline Mn reflects the wider Mn unoccupied LDOS compared to the local LDOS of Mn in NiMnSb. Significant differences exist also in the structurally sensitive regions. The NiMnSb spectrum reveals a deep pronounced minimum followed by a shallow maximum. The spectrum for polycrystalline Mn shows a wide minimum. These differences are attributed to the different crystal structures of both materials. At room termperature, metallic Mn crystallizes in the body centered cubic A12 structure, NiMnSb in the $C1_b$ structure consisting of four fcc lattices shifted along the bulk diagonal of the unit cell by a quarter of its length.

To interpret the NiMnSb spectra in more detail, we performed calculations as described above. A comparison between the experimental (dots) and theoretical spectra (solid line) is shown in Fig. 5(a). The spectra are normalized to equal maximum intensity. The theoretical spectrum is calculated with respect to the Fermi energy. In order to be compared with the experimental spectrum, the calculated spectrum has to be shifted along the energy axis until the peak maxima of the experimental and the theoretical spectra coincide. In our case, the vertical line indicates the Fermi level of the calculation which was shifted by 638.5 eV. This value corresponds to the binding energy[21] of the $Mn2p_{3/2}$ core level. It should be noted that the binding energy measured by
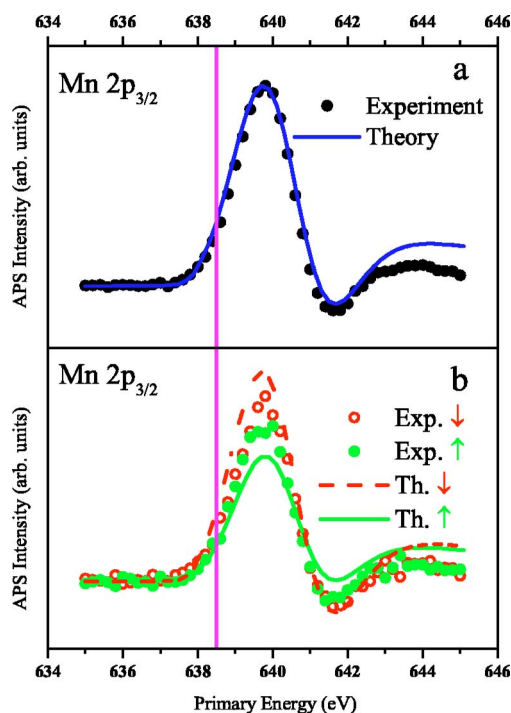
FIG. 5. (Color online) Comparison between experimental (dots) and theoretical (lines) spin-integrated (a) and spin-resolved (b) APS data for NiMnSb(001).

x-ray absorption spectroscopy (XAS) is 639.3 eV (Ref. 39) and by XPS it is 640.2 eV.[15] The differences can be understood in terms of different final states of the different spectroscopies. In the case of XPS the final state consists of a core hole and a fast free electron. In the case of XAS there is a core hole and one additional electron just above E_F. In the case of APS the final state consists of a core hole and two additional electrons just above the Fermi level. Thus, the more electrons the final state contains in the valence band the better the screening of the core hole is. Consequently, the core binding energy measured by the corresponding spectroscopy is lower. As it can be seen from Fig. 5(a), good agreement is achieved between the calculated and the experimental spectrum, thus supporting the chosen values of the parameters within the calculation. Even the structure-sensitive high energy feature above 643 eV is reproduced. The almost quantitative agreement between experiment and theory shows that the LDOS as calculated resembles the Mn LDOS in NiMnSb quite well.

By adding spin resolution, we are able to obtain detailed information about the spin-resolved LDOS. The spin-resolved spectra are shown in Fig. 5(b). The measurements were performed in magnetic remanence after applying an external field of about 800 G along the [110] crystallographic direction. The experimental data for majority spin are presented by filled circles and for minority spin by open circles. With the complex magnetic domain structure in mind, we can expect a reduced and even varying spin asymmetry in the data, depending on which part of the sample is hit by the electron beam. The diameter of the electron beam was ≈ 1 mm, comparable to the laser spot size used for MOKE. Therefore, we investigated different parts of the

sample surface. The spin-resolved spectra in Fig. 5(b) represent an average over many different surface regions. The various spectra with different values for the spin asymmetry were accumulated in such a way that the sign of the spin asymmetry was always the same. The spectra show almost spin-independent line shapes and peak energies. However, the intensity in the minority spectrum is higher than in the majority spectrum, which reflects the higher density of the unoccupied minority states in ferromagnetic NiMnSb.

In addition, Fig. 5(b) shows the calculated spin-resolved APS spectra for $Mn2p_{3/2}$ as dashed and solid lines for the minority and majority channels, respectively. A much higher spin asymmetry in the calculated spectra compared with the experimental data becomes obvious. How can we explain this discrepancy? The spin asymmetry values from APS were found in a range from -0.084 ± 0.020 to 0.034 ± 0.020, depending on the position on the sample where the measurements were performed. To reduce the error bars, these spin asymmetry values were derived not only from the peak maximum but from an interval of 1.2 eV symmetrically around the peak maximum. The variety of values for A can easily be explained by the complex hysteresis loops shown in Fig. 3. Due to the complicated domain structure of the sample at remanence, the SRAPS (and MOKE) measurements integrate over domains with different orientations. Therefore, one can adopt the value of -0.084 ± 0.020 as a lower bound for the spin asymmetry of a magnetic domain in saturation. The mean value for the asymmetry, obtained from the spin-resolved spectra in Fig. 5(b), is -0.064 ± 0.006. The ratio between remanence and saturation differs from place to place on the crystal surface. Therefore, we must divide the mean value for A by 0.56, as determined in Sec. III. In this way we end up with an asymmetry of -0.115 ± 0.012 which is higher than the maximum value of a single measurement. $A = -0.115 \pm 0.012$ is, therefore, an estimated value for A which would be obtained from a NiMnSb sample with saturated magnetization.

From the theoretical spectra we deduce an expected spin asymmetry of $A = -0.25$, taking into account the same energy interval around the peak maxima as described above. This number is two times higher than the experimental result. As a consequence, the complex domain structure with a reduced remanent magnetization is only partly responsible for the discrepancy between the experimentally derived and the theoretically predicted spin asymmetry values. Another reason for the discrepancy might be the different probing depths of MOKE (≈ 200 Å) and APS (≈ 30 Å). We cannot exclude that the surface magnetic properties probed by SRAPS differ from the bulk-like properties probed by MOKE.

An important point is the question whether the bulk electronic structure used in the calculations is maintained within the surface atomic layers probed experimentally. The smaller experimental value for A compared with the calculation may indicate a modified electronic structure at the surface with a reduced magnetization. The fact that the calculated spin-integrated spectrum is in good agreement with the experimental one, while the spin resolved is not, implies very specific changes of the LDOS within the information depth of SRAPS. As mentioned in the Introduction, possible reasons for the reduced spin polarization at E_F and in the unoccupied

states could be found in structural and/or chemical defects at the surface like vacancies, nonideal stoichiometry, or disorder.[40]

Model calculations[41] of chemically disordered NiMnSb crystal demonstrate that the spin polarization at E_F is indeed reduced, but without a significant reduction of the APS asymmetry of the Mn2p signal. Therefore, chemical disorder is not responsible for the reduced asymmetry.

Surface states, as theoretically predicted by Jenkins *et al.*[12] and Wijs *et al.*,[14] may also reduce the polarization and respectively the measured asymmetry. However, they are less relevant to SRAPS measurements. SRAPS as a **k**-integrating technique is not very sensitive to surface states with their small **k**-integrated spectral weight and even not to **k**-dependent changes of the bulk electronic structure. More specific information by spin- and **k**-resolved (inverse) photoemission below as well as above E_F is needed for this purpose. Furthermore, the information depth of ≈ 30 Å for 640 eV electrons used in APS allows only a small contribution of the topmost layer. The same arguments apply to structural defects at the surface.

What remains is a deviation of the surface stoichiometry in the region probed by APS compared to the bulk one. However, our AES data indicate almost perfect bulk stoichiometry at the surface. Taking into account that AES averages over large areas on the sample surface, the overall stoichiometry could be correct but nevertheless the local stoichiometry might differ considerably from the ideal one. An element-specific technique with a high lateral resolution is needed to answer this question.

The former studies on NiMnSb reported in the literature were focused on the half-metallic behavior, i.e., the spin polarization at the Fermi level. Most of the surface/interface sensitive studies reported a reduced spin polarization. Our study provides important new information. It shows a reduced spin polarization of the whole LDOS. This means that modifications of the surface electronic structure compared with the bulk are not restricted to the gap only. The particular reasons for the surface-related changes of the magnetization are not known at present. Yet, we were able to exclude several proposed scenarios to explain this effect.

V. SUMMARY

We have studied the (001) surface of the half-Heusler alloy NiMnSb by means of LEED, AES, MOKE, and SRAPS. The structurally well-ordered ferromagnetic single-crystal surface showed a complex magnetic domain structure at remanence as demonstrated by MOKE. Making use of the surface-sensitive and element-specific spin-resolved appearance potential spectroscopy, we observed a clear spin asymmetry of the local density of unoccupied states for Mn in NiMnSb. A comparison with calculated APS data gives good agreement in the spin-integrated case but not for the spin-resolved data. Even taking into account the magnetic domain structure leaves a factor of 2 between the theoretically predicted and the experimentally measured spin asymmetry. This result demonstrates that the spin-resolved LDOS within the surface region differs from the calculated bulk LDOS.

From a careful analysis of our data, we were able to exclude surface states, chemical disorder, and structural defects as possible reasons for the reduced surface magnetization. Detailed spatial resolved measurements of the local surface morphology as well as **k** and spin-resolved studies of the electronic structure are needed to unveil the origin of the reduced magnetization within the surface region.

[1] G. A. Prinz, Phys. Today **48**, 58 (1995).

[2] P. Ball, Nature (London) **404**, 918 (2000).

[3] P. J. Webster and K. R. A. Ziebeck, *Landolt-Börnstein New Series Group III* (Springer, Berlin, 1988), p. 75.

[4] J. Kübler, A. R. Williams, and C. B. Sommers, Phys. Rev. B **28**, 1745 (1983).

[5] R. A. de Groot, F. M. Mueller, P. G. van Engen, and K. H. J. Buschow, Phys. Rev. Lett. **50**, 2024 (1983).

[6] K. E. H. M. Hanssen, P. E. Mijnarends, L. P. L. M. Rabou, and K. H. J. Buschow, Phys. Rev. B **42**, 1533 (1990).

[7] R. B. Helmholdt, R. A. de Groot, F. M. Mueller, G. P. van Engen, and K. H. J. Buschow, J. Magn. Magn. Mater. **43**, 249 (1984).

[8] F. B. Mancoff, B. M. Clemens, E. J. Singley, and D. N. Basov, Phys. Rev. B **60**, R12565 (1999).

[9] R. J. Soulen, J. M. Byers, M. S. Osofski, B. Nadgorny, T. Ambrose, S. F. Cheng, P. R. Broussard, C. T. Tanaka, J. Nowak, J. S. Moodera, A. Barry, and J. M. D. Coey, Science **282**, 85 (1998).

[10] W. Zhu, B. Sinkovic, E. Vescovo, C. Tanaka, and J. S. Moodera, Phys. Rev. B **64**, 060403(R) (2001).

[11] D. Ristoiu, J. P. Nozieres, C. N. Borca, T. Komesu, H.-K. Jeong, and P. A. Dowben, Europhys. Lett. **49**, 624 (2000).

[12] S. J. Jenkins and D. A. King, Surf. Sci. **494**, L793 (2001).

[13] S. J. Jenkins and D. A. King, Surf. Sci. **501**, L185 (2001).

[14] G. A. de Wijs and R. A. de Groot, Phys. Rev. B **64**, 020402(R) (2001).

[15] C. N. Borca, T. Komesu, H.-K. Jeong, P. A. Dowben, D. Ristoiu, C. Hordequin, J. P. Nozieres, J. Pierre, S. Stadler, and Y. U. Idzerda, Phys. Rev. B **64**, 052409 (2001).

[16] R. L. Park and J. E. Houston, J. Vac. Sci. Technol. **11**, 1 (1974).

[17] U. Kolac, M. Donath, K. Ertl, H. Liebl, and V. Dose, Rev. Sci. Instrum. **59**, 1933 (1988).

[18] D. T. Pierce, R. J. Celotta, G. -C. Wang, W. N. Unertl, A. Galejs, C. E. Kuyatt, and S. R. Mielczarek, Rev. Sci. Instrum. **51**, 478 (1980).

[19] G. Rangelov, K. Ertl, F. Passek, M. Vonbank, S. Bassen, J. Reinmuth, M. Donath, and V. Dose, J. Vac. Sci. Technol. A **16**, 2738 (1998).

[20] M. Donath, Surf. Sci. Rep. **20**, 251 (1994).

[21] J. Reinmuth, F. Passek, V. N. Petrov, M. Donath, V. Popescu, and H. Ebert, Phys. Rev. B **56**, 12893 (1997).

[22] H. Kolev, G. Rangelov, J. Braun, and M. Donath (unpublished).

[23] G. Hörmandinger, P. Weinberger, P. Marksteiner, and J. Redinger, Phys. Rev. B **38**, 1040 (1988).

[24] L. Szunyogh, P. Weinberger, and J. Redinger, Phys. Rev. B **46**, 2015 (1992).

[25] J. Minar, V. Popescu, and H. Ebert, Phys. Rev. B **62**, 10051 (2000).

[26] O. K. Andersen, Phys. Rev. B **12**, 3060 (1975).

[27] O. K. Andersen and O. Jepsen, Phys. Rev. Lett. **53**, 2571 (1984).

[28] K. Ertl, M. Vonbank, V. Dose, and J. Noffke, Solid State Commun. **88**, 557 (1993).

[29] C. Math, J. Braun, and M. Donath, Surf. Sci. **482-485**, 556 (2001).

[30] J. M. Luttinger, Phys. Rev. **121**, 942 (1961).

[31] T. Wegner, M. Potthoff, and W. Nolting, Phys. Rev. B **61**, 1386 (2000).

[32] M. Potthoff, T. Wegner, W. Nolting, T. Schlathölter, M. Vonbank, K. Ertl, J. Braun, and M. Donath, Phys. Rev. B **63**, 165118 (2001).

[33] S. Plogmann, Ph.D. thesis, Universität Osnabrück, 1999.

[34] R. M. Bozorth, *Ferromagnetism* (IEEE Press, New York, 1993), p. 15.

[35] K. Starke, K. Ertl, and V. Dose, Phys. Rev. B **45**, 6154 (1992).

[36] R. L. Park and J. E. Houston, Phys. Rev. B **6**, 1073 (1972).

[37] V. Dose, A. Härtl, J. Rogozik, and H. Warlimont, Solid State Commun. **49**, 509 (1984).

[38] J. Giber, R. Drube, and V. Dose, Appl. Phys. A: Solids Surf. **A52**, 167 (1991).

[39] M. V. Yablonskikh, Y. M. Yarmoshenko, V. I. Grebennikov, E. Z. Kurmaev, S. M. Butorin, L. C. Duda, J. Nordgren, S. Plogmann, and M. Neumann, Phys. Rev. B **63**, 235117 (2001).

[40] D. Orgassa, H. Fujiwara, T. C. Schulthess, and W. H. Butler, Phys. Rev. B **60**, 13237 (1999).

[41] J. Braun (unpublished).